

Thermal conductivities in NaSnAs, NaSnP, and NaSn₂As₂: Effect of double lone-pair electronsZhiping Lin,¹ Gang Wang,¹ Congcong Le,² Huaizhou Zhao,¹ Ning Liu,¹ Jiangping Hu,² Liwei Guo,^{1,*} and Xiaolong Chen^{1,3,4,†}¹Research and Development Center for Functional Crystals, Beijing National Laboratory for Condensed Matter Physics, Institute of Physics, Chinese Academy of Sciences, Beijing 100190, People's Republic of China²Beijing National Laboratory for Condensed Matter Physics, National Laboratory for Superconductivity, Institute of Physics, Chinese Academy of Sciences, Beijing 100190, People's Republic of China³School of Physical Sciences, University of Chinese Academy of Sciences, Beijing 101408, People's Republic of China⁴Collaborative Innovation Center of Quantum Matter, Beijing 100084, People's Republic of China

(Received 19 November 2016; revised manuscript received 19 February 2017; published 14 April 2017)

Materials with low thermal conductivity, which can minimize heat dissipation, play a central role in many practical applications, such as thermoelectric devices and thermal barrier coatings. We report the synthesis and low thermal conductivities of narrow band gap semiconductors NaSnAs and NaSnP, in which the measured minimum lattice thermal conductivities are 0.62 and 0.58 W/m/K. The values are close to the calculated minimum of 0.46 and 0.40 W/m/K, respectively, and obviously lower than that for their closely related compound NaSn₂As₂, which has fewer lone-pair electrons. Such low thermal conductivities in NaSnAs and NaSnP are due to double lone s^2 electron pairs that are present in both Sn sites and As or P sites. Double lone-pair electrons can induce greater Grüneisen parameters γ and lower thermal conductivity further than that in NaSn₂As₂. Our findings provide hints for exploring new materials with low thermal conductivity.

DOI: [10.1103/PhysRevB.95.165201](https://doi.org/10.1103/PhysRevB.95.165201)**I. INTRODUCTION**

Materials with low thermal conductivity are of technological importance in many applications, from thermoelectric devices to thermal insulators [1–4]. As a fundamental property, thermal conductivity reflects the ability of heat transfer by both phonons and electrons in solids. Over the past decades, considerable progress has been achieved in understanding the underlying mechanism for various kinds of compounds that exhibit low thermal conductivity over a certain temperature range. This is, in particular, true for semiconductors and insulators whose thermal conductivity is dominated by phonon contributions. In this regard, typical examples are some chalcogenides such as Cu₇PSe₆ [5], Cu₂S [6], Ag₂Se [7], and Cu₂Se [8,9], with thermal conductivities ranging from 0.1 to 0.6 W/m/K. This class of compounds is the so-called phonon-liquid electron-crystal (PLEC). Their low thermal conductivity is attributed to the existence of local frequency vibrational modes.

Recently, Morelli *et al.* [10] pointed out low conductivity occurs in I-V-VI₂ compounds in which lone electron pairs exist. Then, Skoug and Morelli measured the thermal conductivities in Cu₃SbSe₄, CuSbSe₂, and Cu₃SbSe₃ compounds to discuss the role of lone-pair electrons in producing minimum thermal conductivities [11]. The existence of stereochemically active s^2 orbitals of the group V element (As, Sb, Bi) is thought to be the origin of the strong lattice anharmonicity in the previously mentioned compounds [10–12]. This is manifested by a lower thermal conductivity in CuSbSe₂ than in Cu₃SbSe₄. As 5s electrons for Sb are significantly lower than its 5p electrons in energy, so a weak s - p orbital hybridization prevents the formation of sp^3 bonds and leads to octahedral coordination of Sb by Se in CuSbSe₂. Sb atom

(+3) and Se atom (−2) commonly form polar covalent bonds by sharing p electrons of Sb atom, while the lower energy s^2 electron pair of Sb atom forms lone-pair electrons. In contrast, all of the $5s^25p^1$ valence electrons of Sb atom in Cu₃SbSe₄ participate in forming sp^3 hybrid bonds with Se atom, resulting in a tetrahedral coordination of Sb with Se. Lone-pair electrons are easily deformed in lattice vibrations, leading to a strong anharmonicity due to the nonlinear terms in the total energy associated with a large nonhybrid valence electronic contribution, resulting in low thermal conductivity [12]. This mechanism should also apply to binary compounds such as SnSe [13], PbTe [14], SnTe [15], and Zn₄Sb₃ [16,17] in understanding why they have low thermal conductivities.

Compound NaSnX ($X = \text{As, P}$) contains lone-pair electrons in both Sn and As or P atoms. The role of double lone-pair electrons in affecting thermal conductivity is still unclear. Here, we report on their synthesis and structure, and focus on their thermal conductivities. Both compounds are narrow band gap semiconductors with band gaps about 0.31 and 0.63 eV for NaSnAs and NaSnP, respectively, derived from our density functional theory (DFT) calculations. The measured minimum lattice thermal conductivities of NaSnP and NaSnAs are close to the calculated minimum one and 40% lower than that of their closely related compound NaSn₂As₂, which has fewer lone-pair electrons. It is demonstrated that the large and strong anisotropic Grüneisen parameters induced by anharmonic interaction of doubled lone-pair electrons with phonons is responsible for the low thermal conductivities in NaSnAs and NaSnP. A reduction in number of lone-pair electrons will incur an increase in thermal conductivity.

II. EXPERIMENTAL DETAILS

Sodium lump (Alfa Aesar, 99.7%), tin shot (Alfa Aesar, 99.999%), phosphorus powder (Alfa Aesar, 99.999%), and arsenic lump (Alfa Aesar, 99.99%) were used as starting materials. All manipulations for the sample preparation were

*Corresponding author: lwguo@aphy.iphy.ac.cn†Corresponding author: chenx29@iphy.ac.cn

carried out inside an argon-filled glove box ($O_2 < 1$ ppm and $H_2O < 1$ ppm). NaSnAs, NaSnP, and $NaSn_2As_2$ samples were synthesized by solid-state reactions. The starting materials were first mixed according to the nominal stoichiometric ratio and then sealed in an evacuated silica ampoule back-filled with about 0.2-atm-high pure argon. The ampule was heated to 1123 K in 10 h, followed by keeping at the temperature for 4 h and subsequent cooling to 423 K in 96 h. The products were ground, and the resulting powder was consolidated and sintered under vacuum ($<10^{-3}$ Pa) using spark plasma sintering (SPS) with a pressure of 45 MPa at 773 K for 10 min (soaking time). The samples are 12.7 mm in diameter and around 2 mm in thickness. The densities are 4.26, 3.64, and $5.06 \text{ g}\cdot\text{cm}^{-3}$, corresponding to $\sim 96\%$, $\sim 96\%$, and $\sim 95\%$ of the theoretical ones for NaSnAs, NaSnP, and $NaSn_2As_2$, respectively. Powder x-ray diffraction data (PXRD) obtained on crushed samples were collected at room temperature using a PANalytical diffractometer with Cu $K\alpha$ radiation and a graphite monochromator. Rietveld refinements were performed using the FullProf software package [18]. The chemical compositions of the prepared compounds were characterized by the energy-dispersive x-ray (EDX) spectroscopy. The result for each sample was obtained based on the average of three sets of data. The electrical resistivity and heat capacity measurements were conducted on the Quantum Design Physical Property Measurement System (PPMS). Thermal diffusivities (D) were measured by LFA447 (Netzsch), using discs with a diameter of 12.7 mm and thickness of 2 mm and coated by 10 μm amorphous carbons. Thermal conductivities [19] above room temperature were calculated based on $\kappa = D\rho C_p$, where ρ is the density of the sample, D is the thermal diffusivity, and C_p is the specific heat calculated from the Dulong and Petit law [20]. Linseis LRS-3 was used to measure the electrical transport properties for all samples with dimensions of $2.5 \times 2.5 \times 11 \text{ mm}^3$. The first principles calculations were performed with the Cambridge Serial Total Energy Package (CASTEP) code and the Vienna *Ab initio* Simulation Package (VASP), based on the DFT using Vanderbilt ultrasoft pseudopotentials [21]. The details are shown in the Supplemental Material [22].

III. RESULTS AND DISCUSSION

NaSnAs is a new compound. We find it is isostructural to NaSnP [23]. Figure 1 shows the room temperature PXRD patterns of NaSnAs and NaSnP samples measured from $2\theta = 10^\circ$ to 80° , together with Rietveld refinements on the data. The whole PXRD pattern measured from $2\theta = 10^\circ$ to 130° for NaSnAs is given as Fig. S1 (Supplemental Material [22]), and all crystallographic data are summarized in Table S1 (Supplemental Material [22]). The refined lattice parameters for NaSnP are $a = b = 3.8778(2) \text{ \AA}$ and $c = 11.6657(6) \text{ \AA}$, in good agreement with the previously reported one [23]. Rietveld refinement for NaSnAs was performed against the collected data based on an initial structural model similar to that of NaSnP [23]. The PXRD data for NaSnAs can be well indexed on a hexagonal cell ($P6_3mc$, No. 186) with lattice parameters $a = b = 4.0001(3) \text{ \AA}$ and $c = 11.728(1) \text{ \AA}$. The final agreement factors converge to $R_p = 5.66\%$, $R_{wp} = 7.68\%$, and $R_{exp} = 3.71\%$. Chemical analysis for the

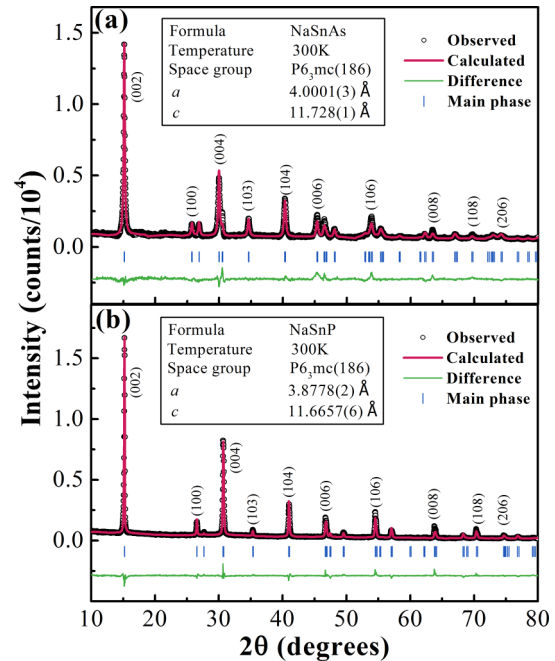


FIG. 1. (a) PXRD pattern collected at 300 K for the NaSnAs and the Rietveld refinement profiles. (b) PXRD pattern collected at 300 K for the NaSnP and the Rietveld refinement profiles.

NaSnAs samples by EDX (see Table S2 in the Supplemental Material [22]) shows that the atomic ratio of Na:Sn:As is 0.99(2):0.99(1):1.03(2), which is close to the stoichiometric atom ratios of NaSnAs. $NaSn_2As_2$ can be well indexed on a trigonal cell ($R\bar{3}m$, No. 166) with lattice parameters $a = b = 4.006(2) \text{ \AA}$ and $c = 27.58(1) \text{ \AA}$ (the PXRD pattern is shown in Fig. S2 in the Supplemental Material [22]), which is consistent with Ref. [24].

The crystal structure of NaSnAs is schematically shown in Fig. 2(a). The Na atoms in the 2b positions are located above the center of each Sn_3As_3 ring [Fig. 2(b)] with an AB stacked sequence. Sn atoms occupy the 2a positions and are coordinated by three As atoms. As atoms occupy the 2b positions and are coordinated by three Sn atoms and three Na atoms. Compared with NaSnAs, $NaSn_2As_2$ [the crystal structure is shown in Figs. 2(c) and 2(d)] contains nearly identical Sn_3As_3 rings, showing an ABB stacked layered structure. The unit cell volume of NaSnAs is larger than that of NaSnP because As atom is larger than P atom (see Table S1 in the Supplemental Material [22]). The average Sn–As distance in NaSnAs is 2.75 \AA , similar to the Sn–P distance in NaSnP (2.82 \AA) and the Sn–As distance in $NaSn_2As_2$ (2.70 \AA) [24], and larger than Sn–As distances in $SnAs_4$ tetrahedral, which are typically in the range of 2.56–2.61 \AA .

The electrical behavior of $NaSn_2As_2$ shows a metallike characteristic [see Fig. S3(c) in the Supplemental Material [22]], which agrees with the result of the first principles calculations (see Fig. S4 in the Supplemental Material [22]). Unlike $NaSn_2As_2$, both NaSnAs and NaSnP exhibit a semiconductor-like characteristic in electrical conductivities at measurement range. The resistivity at room temperature of NaSnAs is six orders lower than that of NaSnP [see Fig. S3(a) and (b) in the Supplemental Material [22]]. A small amount of Sn might

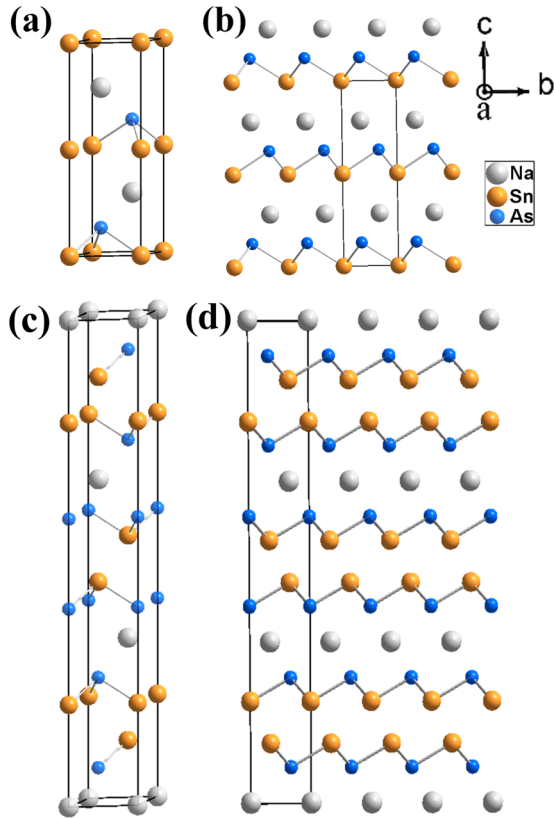


FIG. 2. Crystal structure of NaSnAs and NaSn₂As₂. (a) The schematic crystal structure of NaSnAs. (b) The side view of NaSnAs along *a* axis. (c) The schematic crystal structure of NaSn₂As₂. (d) The side view of NaSn₂As₂ along *a* axis.

be present on the surface of NaSnAs, because it is not stable in air in comparison to NaSnP. But this needs confirmation. The temperature-dependent resistivity for NaSnAs can't be well fitted by a thermal activation model below 235 K. Its active energy gap is estimated to be ~ 16 meV by fitting the data from 235 to 300 K against the Arrhenius formula [see Fig. S3(a) in the Supplemental Material [22]]. Comparatively, NaSnP obeys well the thermal activation model at least for high temperatures (out of measuring range below 240 K). An active energy gap, ~ 250 meV, is obtained by fitting the data above 240 K [see Fig. S3(b) in the Supplemental Material [22]]. The first principles calculations on the band structures in Fig. S4 (Supplemental Material [22]) show that NaSnAs and NaSnP are indirect band gap semiconductors, with gaps ~ 0.31 and 0.63 eV, respectively.

Figure 4(a) represents the temperature dependence of the measured total thermal conductivities κ_{tot} of NaSnAs, NaSnP, and NaSn₂As₂. The measured minimum κ_{tot} of NaSnAs and NaSnP is 0.88 and 0.58 W/m/K at 775 and 825 K, respectively. Since $\kappa_{\text{tot}} = \kappa_{\text{lat}} + \kappa_{\text{ele}}$, the lattice thermal conductivity κ_{lat} can be deduced by subtracting electron thermal conductivity κ_{ele} from κ_{tot} . κ_{ele} is estimated using the Weidemann-Franz law as $\kappa_{\text{ele}} = L_0 \delta T$ [25], where the Lorenz number $L_0 = 2.4 \times 10^{-8} \text{ W}^* \Omega^* \text{ K}^{-2}$, δ is the electrical conductivity of a material, and T is the measurement temperature. The electrical conductivities can be derived from the resistivity of NaSnAs from 300 to 825 K, NaSnP from 650 to 825 K, and

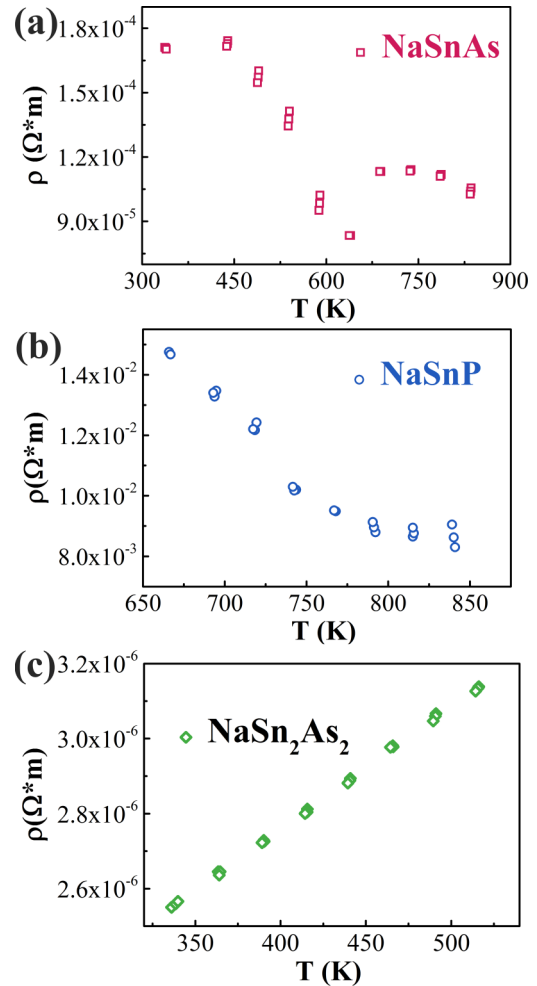


FIG. 3. Dependence of resistivities of NaSnAs, NaSnP, and NaSn₂As₂ on temperature at high temperature. (a) The electrical resistivity vs temperature for NaSnAs from 300 to 825 K. (b) The electrical resistivity vs temperature for NaSnP from 650 to 825 K. (c) The electrical resistivity vs temperature for NaSn₂As₂ from 300 to 515 K.

NaSn₂As₂ from 300 to 515 K (as shown in Fig. 3). The temperature-dependent resistivities of NaSnAs and NaSnP show semiconductor behavior and of NaSn₂As₂ shows metal behavior; these results are consistent with the results measured by PPMS as shown in Fig. S3 (Supplemental Material [22]). For NaSnP, the resistivity is too large to be over the range between 300 and 650 K. The temperature-dependent κ_{lat} for NaSnAs, NaSnP, and NaSn₂As₂ is deduced and displayed in Fig. 4(b). In addition, the maximum contribution of the electron thermal conductivity from NaSnP is less than 1%. All κ_{lat} follow the law $\kappa_{\text{lat}} \approx 1/T$ at the measured temperature range [26]. This indicates that umklapp scattering [27] should be the major scattering mechanism for phonons, as observed in most of the studied crystalline solid materials. However, the κ_{lat} of NaSnAs is nearly half that of its closely related compound NaSn₂As₂.

As is well known, phonon velocity can be used to estimate the high temperature limit for the minimum lattice thermal conductivity. The low Debye temperature is typical for a

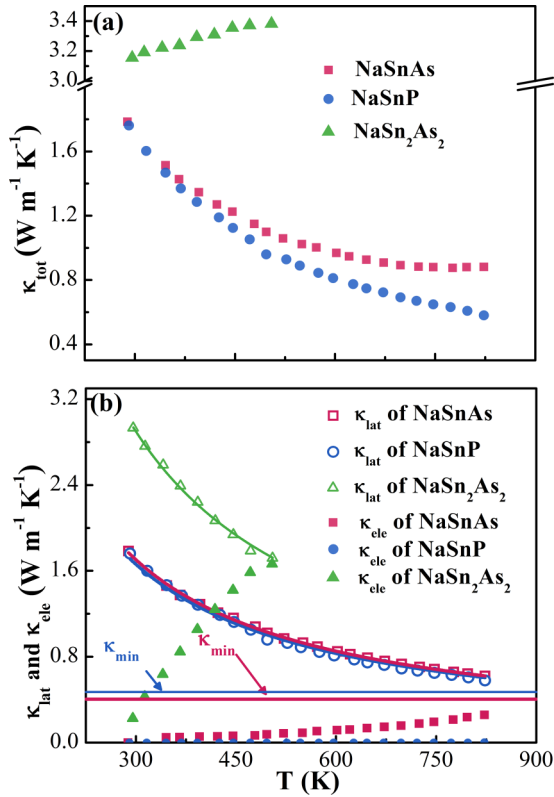


FIG. 4. (a) Total thermal conductivities of NaSnAs, NaSnP, and NaSn₂As₂, respectively. (b) Lattice thermal conductivities of NaSnAs, NaSnP, and NaSn₂As₂ (open symbols) and electron thermal conductivities of NaSnAs and NaSn₂As₂ (filled symbols). All κ_{lat} follow the law $\kappa_{\text{lat}} \propto (1/T)$ (fitting lines) at the measured temperature range. The calculated minimum thermal conductivities κ_{min} of NaSnAs and NaSnP are also shown in solid blue and red lines, respectively, for comparison.

material with a less rigid crystal lattice. Here, based on the Debye model, the Debye temperature of NaSnAs, NaSnP, and NaSn₂As₂ is deduced to be 186, 211, and 193 K from the measured heat capacity (see Fig. S6 in the Supplemental Material [22]). We further estimated the mean phonon velocity v_m using the fitted Debye temperature data via [28] $\Theta = \frac{v_m \hbar}{k_B} \left(\frac{6\pi^2}{V} \right)^{\frac{1}{3}}$, where V is the average volume per atom calculated from the refined lattice parameters, v_m is the calculated average phonon velocity, k_B is the Boltzmann constant, and \hbar is the reduced Planck constant. The calculated average phonon velocity v_m is 1876, 2083, and 1910 m*s⁻¹ for NaSnAs, NaSnP, and NaSn₂As₂, respectively. In comparison, the mean phonon velocities v_m for thermoelectric materials with intrinsic low thermal conductivities are 2310 m*s⁻¹ (β -Zn₄Sb₃) [16,17], 4800 m*s⁻¹ (AgSbTe₂) [11], and 1422, 2002, and 1814 m*s⁻¹, respectively, along a , b , and c axes of SnSe [13]. The value of the so-called minimum thermal conductivity is readily estimated from the formula $\kappa_{\text{lat}} = \frac{1}{3} C_v v_m l$ [29], where the phonon mean free path l is the interatomic spacing, which is 4.000 Å for NaSnAs and 3.878 Å for NaSnP. The isochoric specific heat per mole C_v is approximately equal to the value of the high temperature limit of the specific heat (0.36 J/g/K for NaSnAs, 0.45 J/g/K for NaSnP, and 0.30 J/g/K for NaSn₂As₂). The

calculated minimum thermal conductivities for NaSnAs and NaSnP are 0.40 and 0.46 W/m/K, respectively. We can see that the measured minimum lattice thermal conductivities value of κ_{min} for NaSnAs (0.62 W/m/K) or NaSnP (0.58 W/m/K) is close to the calculated minimum one.

This low κ_{lat} has usually been attributed to the existence of local phonon modes and strong scattering of phonons, which reflects strong anharmonicity in lattices. In this paper, it is reasonable to assume that lone-pair electrons would result in strong anharmonicity and hence reduced lattice thermal conductivities in NaSnAs and NaSnP, as encountered in the thermoelectric materials containing lone-pair electrons [13–16]. A striking feature for NaSnAs and NaSnP is that both contain double lone-pair electrons, unlike the previously reported compounds that have only one lone-pair electron. The Na-Sn-As ternary system presents a unique opportunity to study the effect of double lone-pair electrons on κ_{lat} . Compared with NaSnAs or NaSnP, NaSn₂As₂ contains nearly identical SnAs atom and Na atom layers. According to the Zintl electron count, three coordinated Sn and As atoms tend to fulfill an electron octet by forming three covalent bonds and lone-pair electrons left in Sn atoms and As or P atoms. Thus, the anionic tin-arsenic layer [SnAs]⁻ is negatively charged. Using the ionic approach, assuming a +2 oxidation state for Sn and a -3 oxidation state for As, results in the same charge for the layer (Sn²⁺)(As³⁻) as that from Zintl electron count. In NaSnAs and NaSnP, each SnAs or SnP layer is balanced by a layer of monovalent Na cations. According to Ref. [30], NaSn₂As₂ is not electron balanced, because Na can't donate enough electrons to fill the nonbonding orbitals. There are not enough electrons to form the lone-pair electrons of Sn atom and As atom. In this case, NaSn₂As₂ has fewer lone electron pairs than does NaSnAs.

NaSnAs, NaSnP, and NaSn₂As₂ are expected to have similar κ_{lat} , considering that their average atomic masses are nearly the same and all possess similar chemical bonds. The only reasonable explanation for the large κ_{lat} discrepancy (Fig. 4) is that there must be unaccounted factors that take effect in differentiating κ_{lat} going from NaSnAs to NaSn₂As₂. To probe the discrepancy, we performed analysis of spatial distribution of the difference charge density (DCD) [31–33], including isosurfaces ($\Delta\rho = 0.5$) for NaSnAs, NaSnP, and NaSn₂As, as shown in Fig. 5. Charge difference isosurfaces are obtained by subtracting the free atoms electron densities of Na, Sn, and As or P from that of NaSnAs or NaSnP, namely, $\Delta\rho = \rho_{\text{NaSnAs(P)}} - \rho_{\text{Na}} - \rho_{\text{Sn}} - \rho_{\text{As(P)}}$. The analysis of DCD indicates the presence of charge accumulation due to chemical bonds or lone electron pairs. Examining Fig. 5(b) and (d) reveals a charge accumulation in location 1 that clearly corresponds to covalent bonds between Sn and As or P atoms. In addition, charge accumulations in locations 2 and 3 clearly demonstrate that both Sn and As or P atoms have lone-pair electrons. For NaSnAs, NaSnP, and NaSn₂As₂, As or P has similar coordination to P of PH₃, which is coordinated by 3 Sn atoms in a trigonal pyramidal configuration with an Sn-As(P)-Sn bond angle of 93.4°, 86.9° and 96.7°. PH₃ has lone-pair electrons that mainly come from the 3s electrons of P atoms. For NaSn₂As₂, DCD analysis shown in Fig. 5(f) confirms the expected covalent bonds (charge accumulation 1) between Sn and As atoms, an obvious lone-pair electron near

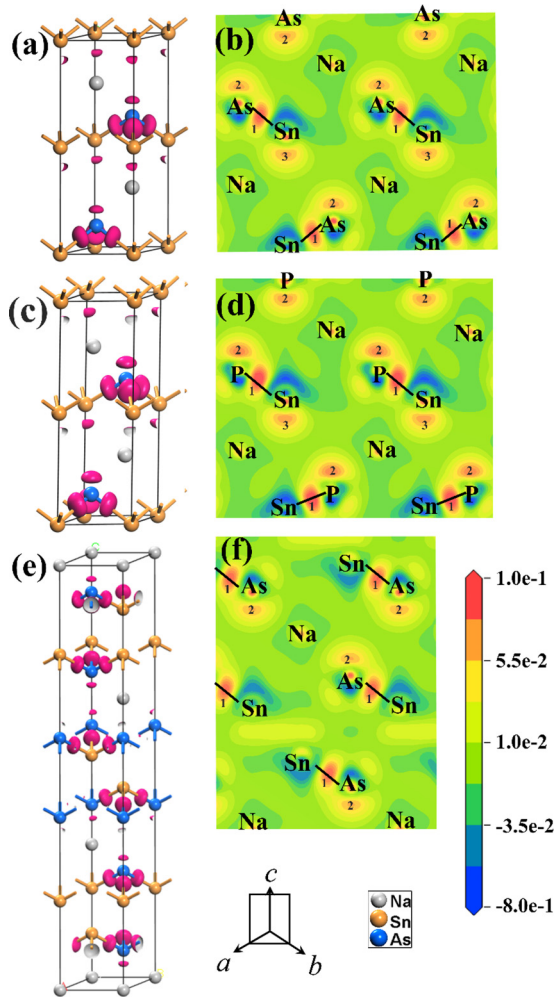


FIG. 5. Isosurfaces of the difference charge density and (110) slices of NaSnAs (a and b), NaSnP (c and d), and NaSn₂As₂ (e and f). Isosurfaces of the difference charge density $\Delta\rho$ expressed with pink areas in (a), (c), and (e) indicate charge accumulation regions, where the density value is about 0.5 electrons/ \AA^3 . The density scale is given in the lower right corner of the figure. The short black lines on (110) slices represent Sn-As or P bonds. The crystallographic axes of a and b and the (110) slice of (b), (d), and (f) are indicated on the bottom.

the As site (charge accumulation 2), and a nearly indiscernible lone-pair electron state near the Sn site. No electron balance in NaSn₂As₂ is responsible for the decrease of lone-pair electrons. Our calculations reveal a strong difference in the lone-pair electrons states for Sn atoms between NaSnAs or NaSnP and NaSn₂As₂. This difference should be the driving force for the discrepancy in Grüneisen parameters.

Double lone-pair electrons in Sn and As or P atoms of NaSnAs and NaSnP are shown schematically in Fig. 6. The lone-pair electrons in Sn atom are toward the positive c axis, and the lone-pair electrons in As atom are toward the negative c axis. These two compounds with double lone-pair electrons are markedly different from the reported materials with only one lone-pair electron. For example, only Sb atoms have the lone-pair electrons in AgSbTe₂ [11], only Sn atoms have them in SnSe [13], and only Pb atoms have them in PbTe [14]. Compared with NaSn₂As₂, the lone s^2 electron pairs of Sn

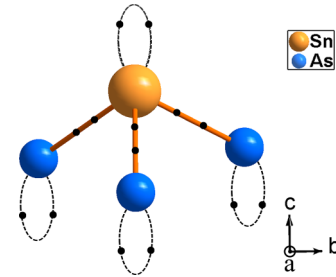


FIG. 6. Schematic representation of the local atomic environments of Sn and As in NaSnAs.

sites and As or P sites are prominent and double, which synergistically favors low intrinsic thermal conductivities of NaSnAs or NaSnP that will equivalently make a significant effect on their Grüneisen parameters.

Now we show how the existence of double lone-pair electrons affects Grüneisen parameter (γ) [34], since it has a direct correlation with thermal conductivity; see the discussion below. Phonon dispersions and Grüneisen parameters of NaSnAs, NaSnP, and NaSn₂As₂ were calculated based on DFT, and all are shown in Table I and Figs. 7 and S5 (see the Supplemental Material [22]). We highlight TA, TA', and LA modes with red, blue, and green in Figs. 7 and S5 (see the Supplemental Material [22]). For these three compounds, strong mixing and highly nonlinear dispersion curves from Γ point to the zone boundary in the acoustic branches resulting from the acoustic branches overlapping with the optical modes. Abrupt changes in the slope of the TA, TA', and LA phonon dispersion come from prevention of crossing between the

TABLE I. Summary of lattice parameters, lattice thermal conductivities, Grüneisen parameters, Debye temperatures, and phonon velocities for NaSnAs, NaSnP, and NaSn₂As₂. The Debye temperature is calculated using $\Theta = \omega_D/k_B$ (ω_D is the largest acoustic frequency in each direction); the phonon velocities v_{TA} , v'_{TA} , and v_{LA} are the slopes of the acoustic phonon dispersion around the point; and \bar{v} is the average phonon velocity.

	NaSnAs	NaSnP	NaSn ₂ As ₂
Space group	$P6_3mc$ (No. 186)	$P6_3mc$ (No. 186)	$R\bar{3}m$ (No. 166)
a (\AA)	4.0001(3)	3.8778(2)	4.006(2)
c (\AA)	11.728(1)	11.6657(6)	27.58 (1)
κ_{lat} (W/m/K)	1.78 (@ 289 K)~	1.76 (@ 291 K)~	2.93 (@ 296 K)~
$\bar{\gamma}$	3.8	3.7	1.5
$\bar{\gamma}_{TA}$	7.2	2.1	1.7
$\bar{\gamma}'_{TA'}$	2.7	5.5	1.7
$\bar{\gamma}_{LA}$	1.7	3.5	1.2
Θ (K)	94	110	100
Θ_{TA} (K)	75	102	85
$\Theta_{TA'}$ (K)	108	103	106
Θ_{LA} (K)	99	126	107
\bar{v} (m*s ⁻¹)	2027	2219	2091
v_{TA} (m*s ⁻¹)	1372	1681	1539
$v'_{TA'}$ (m*s ⁻¹)	1732	1893	1740
v_{LA} (m*s ⁻¹)	2977	3150	2994

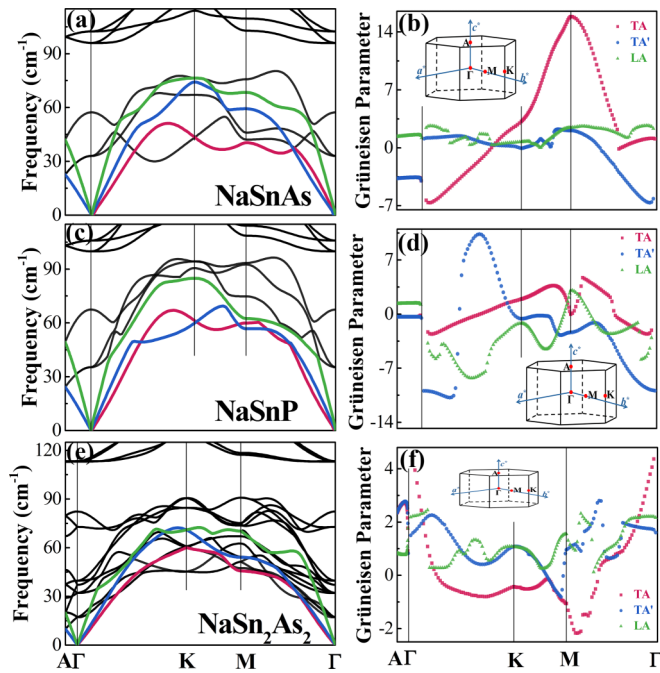


FIG. 7. Phonon dispersions and corresponding acoustic Grüneisen parameters of NaSnAs (a and b), NaSnP (c and d), and NaSn₂As₂ (e and f). The curves expressed by red, blue, green, and black represent the TA, TA', LA, and optical modes, respectively. The insets are the first Brillouin zones of the compounds with high-symmetry points.

optical and the acoustic modes, as reported in Ref. [3]. Looking into the variation of γ in the Brillouin zone, we find that γ are more anisotropic in the former two compounds than in the latter one, as shown in Figs. 7(b), 7(d), and 7(f). We then calculate the average Grüneisen parameter ($\bar{\gamma}$) of each acoustic dispersion ($\bar{\gamma} = \sqrt{\langle \gamma_i^2 \rangle}$). In NaSnAs and NaSnP, $\bar{\gamma}_{TA}$, $\bar{\gamma}'_{TA}$, and $\bar{\gamma}_{LA}$ differ greatly (Table I), and the averaged $\bar{\gamma}$ of them is around 3.8 and 3.7, respectively. However, for NaSn₂As₂, $\bar{\gamma}_{TA}$, $\bar{\gamma}'_{TA}$, and $\bar{\gamma}_{LA}$ are nearly identical and the averaged $\bar{\gamma}$ is around 1.5, which is obviously lower to the values for NaSnAs and NaSnP. Table I summarizes the $\bar{\gamma}$ values, lattice thermal conductivities, and lattice parameters for these three compounds. In comparison, the averaged $\bar{\gamma}$ for thermoelectric materials with intrinsic low thermal conductivities are 1.57 (β -Zn₄Sb₃) [16,17] and 2.05 (AgSbTe₂) [11]. We further evaluate and summarize the Debye temperatures and their corresponding phonon velocities in Table I. The calculated Debye temperatures by DFT for

these three compounds are smaller than our experimental values from using the Debye model. The difference results from avoided crossing between acoustic branches and optical modes. Phonon dispersions and the calculated phonon velocities (2027 m*s⁻¹ for NaSnAs, 2219 m*s⁻¹ for NaSnP, and 2091 m*s⁻¹ for NaSn₂As₂) are close to values deduced from specific heat measurements (1876 m*s⁻¹ for NaSnAs, 2083 m*s⁻¹ for NaSnP, and 1910 m*s⁻¹ for NaSn₂As₂).

Lattice thermal conductivity is known to be connected to the Grüneisen parameter in solids by $\kappa_{\text{lat}} = 3.5 \left(\frac{k_B}{h}\right)^3 \frac{\bar{M} V^{1/3} \theta^3}{\gamma^2 T}$ [27], where V is the volume per atom and \bar{M} is the average mass of atoms in the crystal. The low κ_{lat} has usually been attributed to contributions from the crystal structure, the low Debye temperature, and strong anharmonicity, which is in inverse proportion to γ^2 . To a simple harmonic vibration, the value of γ is zero. The stronger the anharmonicity, the larger the value of γ . Thus, γ provides a convenient way to estimate the anharmonicity in a compound [35]. The amount of double lone-pair electrons per unit cell for NaSnAs and NaSnP is more than that of NaSn₂As₂. This explains why the former two compounds have lower conductivities than NaSn₂As₂ does.

IV. SUMMARY

In summary, we report the synthesis, structures, and thermal conductivities of NaSnAs, NaSnP, and their closely related compound NaSn₂As₂. It is found that the thermal conductivity in NaSnAs or NaSnP is 40% lower than in NaSn₂As₂. Lower thermal conductivities of NaSnAs and NaSnP are attributed to the strong anharmonicity due to double lone-pair electrons that gives rise to high Grüneisen parameters. We demonstrate that the double lone s^2 electron pairs of Sn sites and As or P sites synergistically result in thermal conductivity of NaSnAs or NaSnP far lower than NaSn₂As₂. Our results suggest that low thermal conductivity occurs in compounds with more lone electron pairs in each unit cell, which could serve as a guide for searching compounds with low thermal conductivity.

ACKNOWLEDGMENTS

This paper was partly supported by the National Natural Science Foundation of China (Grants No. 51532010, No. 91422303, No. 51322211, and No. 11334012), the Strategic Priority Research Program of the Chinese Academy of Sciences (Grant No. XDB07000000), and the Ministry of Science and Technology of China 973 program (Grant No. 2015CB921300).

- [1] C. B. Vining and D. Rowe, in *CRC Handbook of Thermoelectrics*, edited by D. M. Rowe (CRC Press, Boca Raton, FL, 1995).
- [2] S. Ballikaya, H. Chi, J. R. Salvador, and C. Uher, *J. Mater. Chem. A* **1**, 12478 (2013).
- [3] J. R. Sootsman, D. Y. Chung, and M. G. Kanatzidis, *Angew. Chem. Int. Ed.* **48**, 8616 (2009).
- [4] G. J. Snyder and E. S. Toberer, *Nat. Mater.* **7**, 105 (2008).
- [5] K. S. Weldert, W. G. Zeier, T. W. Day, M. Panthöfer, G. J. Snyder, and W. Tremel, *J. Am. Chem. Soc.* **136**, 12035 (2014).
- [6] Y. He, T. Day, T. Zhang, H. Liu, X. Shi, L. Chen, and G. J. Snyder, *Adv. Mater.* **26**, 3974 (2014).
- [7] M. Ferhat and J. Nagao, *J. Appl. Phys.* **88**, 813 (2000).
- [8] H. Liu, X. Shi, F. Xu, L. Zhang, W. Zhang, L. Chen, Q. Li, C. Uher, T. Day, and G. J. Snyder, *Nat. Mater.* **11**, 422 (2012).
- [9] H. Liu, X. Yuan, P. Lu, X. Shi, F. Xu, Y. He, Y. Tang, S. Q. Bai, W. Q. Zhang, L. D. Chen, Y. Lin, L. Shi, H. Lin, X. X. Gao, X. M. Zhang, H. Chi, and C. Uher, *Adv. Mater.* **25**, 6607 (2013).
- [10] D. T. Morelli, V. Jovovic, and J. P. Heremans, *Phys. Rev. Lett.* **101**, 035901 (2008).

- [11] E. J. Skoug and D. T. Morelli, *Phys. Rev. Lett.* **107**, 235901 (2011).
- [12] M. D. Nielsen, V. Ozolins, and J. P. Heremans, *Energ. Environ. Sci.* **6**, 570 (2013).
- [13] L.-D. Zhao, S.-H. Lo, Y. Zhang, H. Sun, G. Tan, C. Uher, C. Wolverton, V. P. Dravid, and M. G. Kanatzidis, *Nature* **508**, 373 (2014).
- [14] J. P. Heremans, V. Jovovic, E. S. Toberer, A. Saramat, K. Kurosaki, A. Charoenphakdee, S. Yamanaka, and G. J. Snyder, *Science* **321**, 554 (2008).
- [15] H. Fleischmann, O. G. Folberth, and H. Pfister, *Z. Naturforsch. A* **14A**, 999 (1959).
- [16] T. Caillat, J.-P. Fleurial, and A. Borshchevsky, *J. Phys. Chem. Solid.* **58**, 1119 (1997).
- [17] G. J. Snyder, M. Christensen, E. Nishibori, T. Caillat, and B. B. Iversen, *Nat. Mater.* **3**, 458 (2004).
- [18] J. Rodríguez-Carvajal, *Phys. B* **192**, 55 (1993).
- [19] W. J. Parker, R. J. Jenkins, C. P. Butler, and G. L. Abbott, *J. Appl. Phys.* **32**, 1679 (1961).
- [20] L. D. Landau and E. M. Lifshitz, *Statistical Physics*, part I (Pergamon, Oxford, UK, 1980).
- [21] S. J. Clark, M. D. Segall, C. J. Pickard, P. J. Hasnip, M. I. J. Probert, K. Refson, and M. C. Payne, *Z. Kristallogr.* **220**, 567 (2005).
- [22] See Supplemental Material at <http://link.aps.org/supplemental/10.1103/PhysRevB.95.165201> for the PXRD pattern of NaSnAs in Fig. S1, Rietveld refinement parameters for NaSnAs and NaSnP in Table S1, EDX results of NaSnAs and NaSnP in Table S2, PXRD pattern of NaSn₂As₂ in Fig. S2, and resistivities at low temperature, electronic band structure, electronic state densities, and phonon dispersions heat capacities of NaSnAs, NaSnP, and NaSn₂As₂ in Figs. S3–S6.
- [23] B. Eisenmann and U. Roessler, *Z. Kristallogr.-New Cryst. Struct.* **213**, 28 (1998).
- [24] M. Asbrand, B. Eisenmann, and J. Klein, *Z. Anorg. Allg. Chem.* **621**, 576 (1995).
- [25] W. Jones and N. H. March, *Theoretical Solid State Physics: Perfect Lattices in Equilibrium* (Courier Dover Publisher, New York, NY, 1973).
- [26] H. Kitagawa, M. Wakatsuki, H. Nagaoka, H. Noguchi, Y. Isoda, K. Hasezaki, and Y. Noda, *J. Phys. Chem. Solid.* **66**, 1635 (2005).
- [27] T. M. Tritt, *Thermal Conductivity: Theory, Properties, and Applications* (Springer Science & Business Media, Berlin, Germany, 2005).
- [28] O. L. Anderson, *J. Phys. Chem. Solid.* **24**, 909 (1963).
- [29] C. Kittel and D. F. Holcomb, *Am. J. Phys.* **35**, 547 (1967).
- [30] M. Q. Arguilla, J. Katoch, K. Krymowski, N. D. Cultrara, J. S. Xu, X. X. Xi, A. Hanks, S. S. Jiang, R. D. Ross, R. J. Koch, S. Ulstrup, A. Bostwick, C. Jozwiak, D. W. McComb, E. Rotenberg, J. Shan, W. Windl, R. K. Kawakami, and J. E. Goldberger, *ACS Nano* **10**, 9500 (2016).
- [31] M. C. Payne, M. P. Teter, D. C. Allan, T. Arias, and J. Joannopoulos, *Rev. Mod. Phys.* **64**, 1045 (1992).
- [32] W. Kohn and L. J. Sham, *Phys. Rev.* **140**, A1133 (1965).
- [33] P. Hohenberg and W. Kohn, *Phys. Rev.* **136**, B864 (1964).
- [34] M. T. Dove, *Structure and Dynamics: An Atomic View of Materials* (Oxford University Press, Oxford, UK, 2003).
- [35] Y. Zhang, E. Skoug, J. Cain, V. Ozolins, D. Morelli, and C. Wolverton, *Phys. Rev. B* **85**, 054306 (2012).